

Continuum Manipulator with Redundant Backbones and Constrained Bending Curvature for Continuously Variable Stiffness

Bin Zhao, Weihao Zhang, Zhaoyu Zhang, Xiangyang Zhu, *Member, IEEE*, and Kai Xu*, *Member, IEEE*

Abstract—Snake-like manipulators can navigate and perform manipulation in confined spaces. Their recent implementations in surgical robots attracted a lot of attentions. These slender manipulators usually possess either a hyper-redundant articulated vertebrate structure or a continuum one. Primary design considerations usually converge to a balance between proper workspace and acceptable stiffness. Efforts have hence been constantly made to achieve higher or adjustable stiffness for a manipulator to widen its applications. This paper presents a simple continuum manipulator design with variable stiffness based on redundantly arranged elastic backbones and continuously constrained bending curvature. The design concepts, kinematics, a preliminary formulation for stiffness adjustment, system construction and experimental characterizations are elaborated. The results showed that the manipulator's stiffness can be increased up to 4.71 times of the value without the curvature constraining rod, indicating the efficacy of the proposed idea.

I. INTRODUCTION

Snake-like manipulators have been of interest for their dexterity and functionality in confined spaces. Recent implementations of these slender manipulators with various structures and miniature sizes in surgical robots attracted a lot of attentions, as they can be deployed to deep surgical sites for interventions through natural orifices or small skin incisions [1]. Other useful applications of these slender manipulators include rescue, inspection and manipulation tasks in a complex environment or in a cavity [2-4]. These slender manipulators have either a continuum structure [5, 6] or an articulated hyper-redundant vertebrate one.

While designing such a slender manipulator, the primary considerations often focus on finding a balance between its workspace and stiffness [1, 5]. Given a desired manipulator diameter, a bigger workspace usually needs a slimmer (a.k.a., longer) structure and hence a lower stiffness (possibly with a smaller payload capability). Many techniques have hence been introduced for stiffness adjustments.

- In the friction-based approaches, the stiffness is changed

essentially by changing the interaction, hence friction, between various structural members. Typical techniques include i) changing the actuation tendon tensions [7-11]; and ii) introducing a pressure/vacuum induced jamming [12-15]. These techniques can be further enhanced by specially routing the tendons [10] or creating matching surface patterns [12].

- Activatable materials (e.g. magnetorheological fluids [16], electrorheological fluids [17] or thermally softened alloy or plastics [18, 19]) can be integrated to vary the structural stiffness while activated by applied external fields.
- It is also possible to adjust stiffness via structure variations, including i) inserting stiffening components [20], and ii) connecting rigid components into the manipulator structure serially [21] or in parallel [22].
- In the analytical approaches, stiffness control can be achieved by i) driving a continuum manipulator into different poses [23] upon understanding its mechanics [24-26], or ii) designing a stiffness controller [27] upon the realization of its force sensing capability [28, 29].

The friction-based approaches pose two main drawbacks: i) the difficulty of realizing continuous stiffness adjustment due to the sudden change in the friction coefficient when static friction turns into sliding one, and ii) possible actuation hysteresis due to the purposely introduced friction. On the other hand, the uses of activatable materials and/or structural variations usually lead to considerable increase in the system complexity. Besides, the response can be slow for the heat-activated plastics. Meanwhile, the analytical approaches can be challenging in formulating the stiffness model based on the continuum mechanics with possible discrepancy between the models and the constructed systems.

This paper hence proposes a simple design for variable stiffness on a continuum manipulator. The proof-of-concept prototype consists of a 2-segment continuum arm and an actuation unit, as in Fig. 1. Its stiffness adjustment is achieved via redundant arrangement of multiple elastic backbones and continuous constraint of the segments' bending curvature.

Contributions of this work hence lie on the proposed design and a preliminary formulation for stiffness adjustment. The effectiveness was verified by a series of experiments. A minor contribution is the design of the curvature-constraining tube as a key component that enables the whole idea.

This paper is organized as follows. Section II explains the design concepts, differentiating the proposed idea from existing similar ones. The prototype design and construction are presented in Section III. Section IV presents the kinematic

Manuscript received Feb 28th, 2018. This work was supported in part by the National Natural Science Foundation of China (Grant No. 51435010, Grant No. 51722507 and Grant No. 91648103), and in part by the National Key R&D Program of China (Grant No. 2017YFC0110800).

Kai Xu, Weihao Zhang and Xiangyang Zhu are with School of Mechanical Engineering, Shanghai Jiao Tong University, Shanghai, China (asterisk indicates the corresponding author, phone: 86-21-34206547; emails: k.xu@sjtu.edu.cn, zwh0813@sjtu.edu.cn, mexyzhu@sjtu.edu.cn).

Bin Zhao and Zhaoyu Zhang are with the RII Lab (Lab of Robotics Innovation and Intervention), UM-SJTU Joint Institute, Shanghai Jiao Tong University, Shanghai, China (emails: zhaobin2014@sjtu.edu.cn and zhangzhaoyu@sjtu.edu.cn).

model and a preliminary formulation for stiffness adjustment. The experimental characterizations are presented in Section V, with the conclusions and future works summarized in Section VI.

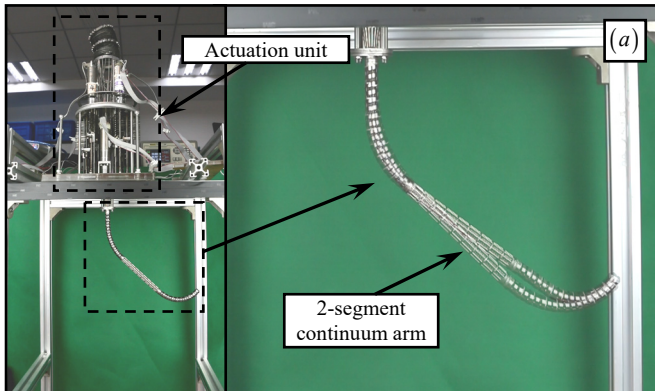


Fig. 1. The constructed continuum manipulator with variable stiffness: (a) differently constrained curvature overlaid while reaching the same position

II. DESIGN CONCEPTS

This study proposes a variable stiffness design for a continuum manipulator using two concepts as introduced in Section II.A and Section II.B respectively. The proposed approach doesn't complicate the manipulator structure and can adjust the stiffness within a wide range.

A. Constrained Bending Curvature

The first concept is to constrain the bending curvature of a continuum segment as shown in Fig. 2.

Such a continuum segment shown in Fig. 2(a) can be used to form a multi-DoF (Degree of Freedom) manipulator as in Fig. 1. The segment consists of i) an end ring, ii) several spacer rings, iii) a base ring, and iv) several backbones. The backbones are made from super-elastic nitinol rods or tubes. They are connected to the end ring and can slide in the holes of the base and the spacer rings.

Bending of the segment is achieved via simultaneously pushing and pulling these backbones. The backbones are not addressed as tendons because they can be pulled and pushed. A tendon usually can only be pulled. The segment's bent shapes can be approximated as circular arcs according to previous analytical and experimental studies [28, 30].

The proposed idea is to insert a rod or tube inside the segment to change the effective length of the segment. This length change will lead to the changes in the segment's potential energy and energy gradient as so to achieve stiffness adjustments. This approach is analog to the fact that a shorter cantilever appears to be more rigid.

The curvature-constraining rod (or tube) can be straight or curved. It should be rigid (or substantially stiffer than the continuum segment). Please note that its role is different from a stiffening rod used in [20]. The curvature-constraining rod changes the effective segment length so as to change the segment stiffness. The proposed approach is also different from the use of the serially connected rigid links in [21] where the segment lengths do not change. The use of the

curvature-constraining rod here is also different from its use in [31] where the bending was constrained to generate different kinematics.

According to the modeling assumptions in Section IV.A, when a straight rod is inserted inside the segment, the orientation of the end ring would remain the same but the position would be altered, as shown in Fig. 2. The change in the end ring position is handled by the kinematics of the 2-segment continuum arm as detailed in Section IV.C.

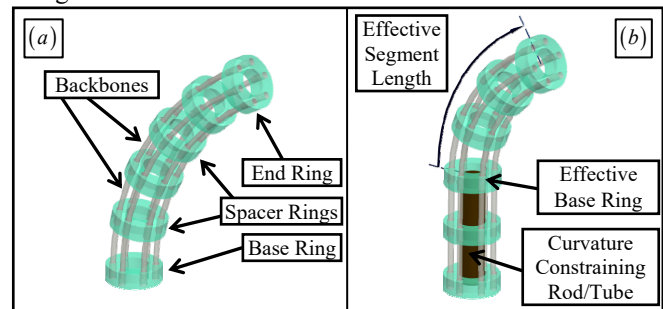


Fig. 2. Alter the stiffness by changing the bending curvature

It should also be noted that the change of the effective segment length is close to a continuous one. It might be perceived from Fig. 2(b) that the change is discrete from one ring to another. As explained in Section III.A, a continuous surface between the rings and the rod is incorporated in the manipulator design to facilitate the rod insertion as well as change the effective segment length gradually.

B. Redundant Backbone Arrangement

The curvature-constraining rod provides a fine adjustment of the stiffness, while the dual continuum mechanism concept provides the adjustments over a range.

The dual continuum mechanism was proposed in [32]. It consists of i) a distal segment (DS), ii) a proximal segment (PS), and iii) guiding cannulae, as shown in Fig. 3(a). The DS and the PS are both structurally similar to the one in Fig. 2(a). The backbones are routed from the DS through the cannulae to the PS, connecting the end rings of the DS and the PS.

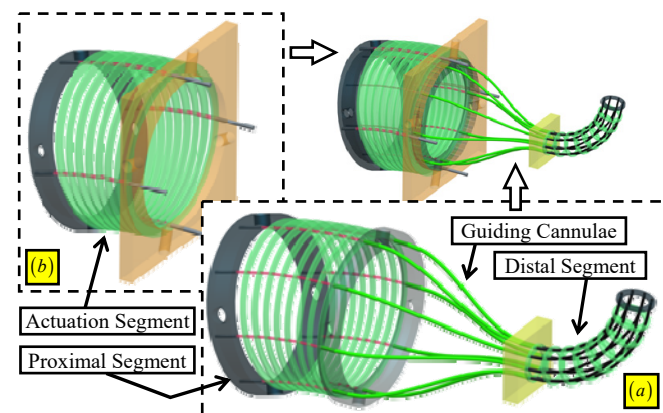


Fig. 3. One (a) dual continuum mechanism with (b) an actuation segment

Backbone arrangements in the DS and the PS shall be kept similar. Then as explained by the kinematics in Section IV.B, bending the PS always bends the DS in the opposite direction, no matter how many backbones are arranged in the segments.

The PS of a dual continuum mechanism can be assembled

into an actuation segment (AS, as in Fig. 3) for actuation.

The structure of the dual continuum mechanism enables actuation modularity and stiffness variation. The DS can be designed for different lengths and sizes, and with different backbone arrangements. As far as the PS can be assembled into the same AS, all the DSs can be consistently actuated. A minimum of three or a large number of backbones can be used. This can change the DS's stiffness over a large range.

Two or more DSs can be stacked to form a multi-DoF continuum manipulator, actuated by the same number of stacked PSs and ASs.

III. DESIGN DESCRIPTIONS OF THE MANIPULATOR

The continuum manipulator with variable stiffness consists of a 2-segment continuum arm shown in Fig. 4(a) and an actuation unit. Besides bending the continuum segments, the actuation unit also constrains the bending curvature of the segments. The system components together with the control infrastructure are elaborated.

A. 2-Segment Continuum Arm

The schematic of the 2-segment continuum arm is shown in Fig. 4(b). The two distal segments (referred to as DS-1 and DS-2 in Fig. 4) are serially connected. They are actuated by two proximal segments (shown in Fig. 5) using the dual continuum mechanism concept from Section II.B.

Each DS possesses eight nitinol backbones. The spacer rings were welded on a helical strip to be apart from one another. The helical strip was wrapped on the surfaces of the DS-1 and DS-2, as in Fig. 4(a). A stainless steel braided tube is fixed inside the spacer rings to provide a smooth surface for the insertion of the curvature-constraining rods.

Two methods are used for stiffness variation.

The first is a redundant arrangement of the backbones. No matter how many backbones are arranged in the DSs, the PSs can always actuate the DSs consistently following the concept of the dual continuum mechanism. As shown in a previous study [22], a segment's stiffness can be increased four times when the number of backbones is increased from 3 to 18. Similar stiffness variations are also expected here. Please note that this aspect only provides stiffness variation during the design stage of the manipulator.

The second is to constrain the bending curvature. The curvature-constraining rods inside the DS-1 and DS-2 are referred to as CC rod-1 and CC rod-2, respectively, as shown in Fig. 4(b). The CC rod-1 and the CC rod-2 are inserted into the DSs to change the length of the bent portion so as to constrain the DSs' bending curvature.

A key enabling component for the idea of curvature constraining is to allow the translation of the CC rod-2 inside the DS-2 without influencing the DS-1. Here a jointed chain structure was designed as shown in Fig. 4(c). The jointed chain is composed of articulated links that are cut from a tube using wire EDM (Electrical Discharge Machining), as shown in Fig. 4(d). Adjacent chain links form revolute joints with $\pm 15^\circ$ rotation range and rotation axes perpendicularly

arranged with respect to each other. The jointed chain has high axial rigidity for transmitting pushing and pulling, while it has low bending stiffness (close to zero) for not affecting the DSs' bending.

The jointed chain is connected with the CC rod-2 so that the actuation unit translates the jointed chain to push or pull the CC rod-2. On the other hand, the actuation unit directly drives the CC rod-1 for the DS-1. Please note that the CC rod-1 moves inside the jointed chain for the CC rod-2. For structural consistency of DSs, a similar jointed chain is also integrated inside the DS-2, as shown in Fig. 4(b).

The rigid portion of the DS-2 in Fig. 4(a) houses the CC rod-2 as shown in Fig. 4(c) to give the maximal bending length of the DS-2. This rigid portion has to be long enough so that the DS-2's effective length can be changed properly.

The jointed chain has an outer diameter of 7mm and an inner diameter of 6 mm, while the CC rods both have an outer diameter of 5.5 mm.

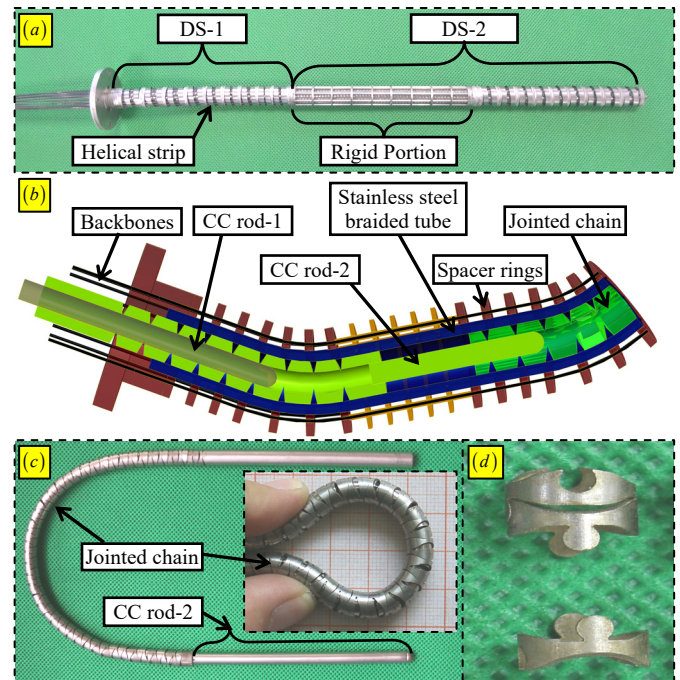


Fig. 4. The 2-segment continuum arm: (a) the actual arm, (b) the schematic, and (c) the jointed chain with the CC rod-2, and (d) the chain links

B. Actuation Unit

The actuation unit in Fig. 5 consists of the driving assembly for the PSs, and the driving assembly for the CC rods.

In this design, the ASs from Section II.B are merged with the PSs. Namely for each PS, four actuation backbones that are arranged 90° apart are attached to the end ring. According to the kinematics in Section IV.B, the pair of the actuation backbones on the opposite sides of the PS shall be pushed and pulled for the same amount to bend the PS.

There are two DSs in the continuum arm. Then two PSs shall be actuated. In total eight actuation backbones for the PS-1 and PS-2 are pushed and pulled by four pair of lead screws. Each pair of lead screws is coupled via a meshing pair of spur gears. In this way, the nuts translate in the opposite direction with the same amount. The actuation backbones are

fixed to the nuts, passing through a few cannulae. Both the nut and a square bellow slide on the guiding rods. The square bellow prevents the actuation backbone from buckling under pushing forces.

The CC rod-2 is actuated by the jointed chain that is driven by another lead screw, as shown in Fig. 5(c). The CC rod-1 moves inside the jointed chain for the CC rod-2. In order to arrange the motors in a compact way, two bars were used to connect the CC rod-1 and the nut for translational actuation.

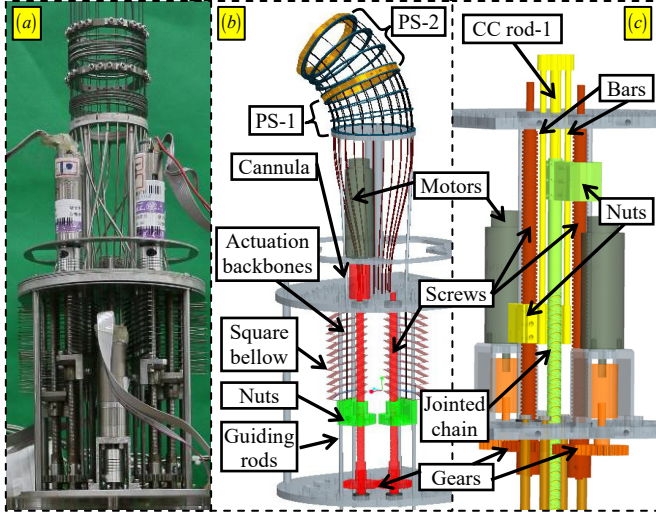


Fig. 5. The actuation unit (a) the actual prototype, (b) the driving assembly for the PSs, and (c) the driving assembly for the curvature-constraining rods

C. Control Infrastructure

Six servomotors were used to drive the 2-segment continuum arm with variable stiffness (four for bending and two for curvature constraining). These Maxon DCX22L servomotors are with the GPX-22 gearheads (gear ratio of 21:1) and the ENX16 encoders with 512 CPT (Counts per Turn). Six Maxon EPOS2 24/2 digital controllers were used to control the servomotors. The actuation kinematics is implemented in a desktop computer and the desired positions for the servomotors are transmitted from the computer to the EPOS2 controllers via a CAN (Controller Area Network) bus.

IV. KINEMATICS AND STIFFNESS CONTROL

The nomenclature, the coordinates and the modeling assumptions are presented in Section IV.A. Kinematics of a curvature-constrained segment is derived in Section IV.B. The model is applicable to all the DSs due to the structural similarity. The kinematics of the 2-segment continuum manipulator is derived in Section IV.C, whereas a preliminary stiffness adjustment formulation is presented in Section IV.D.

A. Nomenclature, Coordinates and Modeling Assumptions

The nomenclature and the coordinates are hence defined for the t th segment, as in Table I and Fig. 6.

- **Base Ring Coordinate** $\{tb\} \equiv \{\hat{x}_{tb}, \hat{y}_{tb}, \hat{z}_{tb}\}$ is attached to the base ring with its origin at the ring's center. \hat{x}_{tb} points from the center to the first backbone.
- **Constrained Base Ring Coordinate** $\{tc\} \equiv \{\hat{x}_{tc}, \hat{y}_{tc}, \hat{z}_{tc}\}$ is

attached to a virtual spacer ring whose position is determined by the insertion of curvature-constraining rod and it indicates the bent portion of the t th segment. Following the modeling assumptions, $\{tc\}$ is continuously translated from $\{tb\}$ in the \hat{z}_{tb} direction, given a straight curvature-constraining rod.

- **Bending Plane Coordinate-1** $\{tp\} \equiv \{\hat{x}_{tp}, \hat{y}_{tp}, \hat{z}_{tp}\}$ shares its origin with $\{tc\}$ and has the bent portion of the t th segment bent in its XY plane.
 - **Bending Plane Coordinate-2** $\{tu\} \equiv \{\hat{x}_{tu}, \hat{y}_{tu}, \hat{z}_{tu}\}$ is obtained from $\{tp\}$ by a rotation about \hat{z}_{tp} such that \hat{x}_{tu} becomes the virtual backbone tangent at the end ring of the t th segment.
 - **End Ring Coordinate** $\{te\} \equiv \{\hat{x}_{te}, \hat{y}_{te}, \hat{z}_{te}\}$ is fixed to the end ring of the t th segment. \hat{x}_{te} points from the center to the first backbone and \hat{z}_{te} is normal to the end ring.
- Three modeling assumptions are used.
- The backbones are pushed and pulled to bend the segment. A virtual backbone in the center as shown in Fig. 6 indicates the segment's length and shape. It is assumed that the rings are always perpendicular to the virtual backbone. Shapes of the backbones can be described by a sweeping motion of a ring (representing the cross section) along the virtual backbone.
 - Shapes of the segment's bent portion can be approximated as circular arcs according to the previous analytical and experimental studies [28, 30]
 - The curvature-constraining rods can be inserted to change the length of the segment's bent portion continuously.

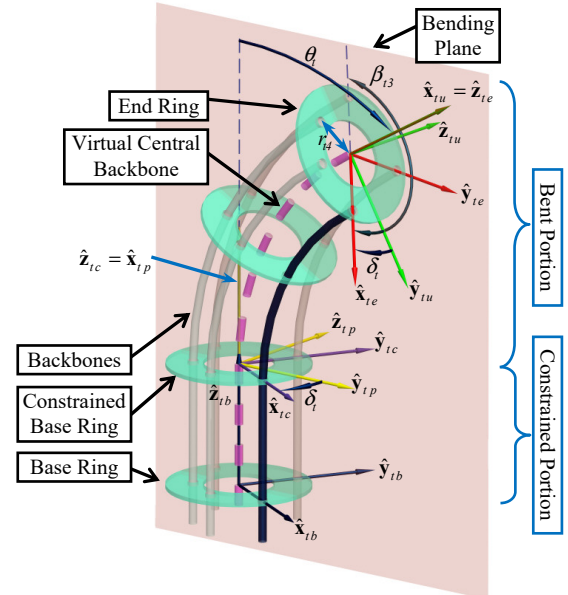


Fig. 6. Nomenclature and coordinates of the curvature-constrained segment

TABLE I
NOMENCLATURE USED IN THIS PAPER

Symbol	Definition
t	Index of the segments, $t = 1$ or 2 . Symbols with a subscript t indicate that the symbols are defined for the t th segment.
i	Index of the backbones, $i = 1, 2, \dots, m$. Numbering of the

	segments always precedes that of the backbones.
r_{ii}	Distance from the virtual backbone to the i th backbone
β_{ii}	Division angle from the i th backbone to the l st backbone; $\beta_{ii}=0$ and β_{ii} remain constant once the segment is built.
l_{bt}	Length of the t th segment measured from the base ring to the end ring along the virtual backbone
l_{ct}	Length of the segment's bent portion measured from the constrained base ring to the end ring along the virtual backbone
ρ_t	Radius of curvature of the t th segment's bent portion
δ_t	A right-handed rotation angle from $\hat{y}_{t,p}$ to $\hat{x}_{t,c}$ about $\hat{z}_{t,c}$.
$\theta_t(s)$	Slope angle of the tangent to the central virtual backbone along its length s in the bending plane. Under the circular bending assumption, this angle at the virtual backbone's tip is enough to describe the segment's bent shape and it is designated as θ_t .
Ψ_t	$\Psi_t \equiv [\theta_t, \delta_t, \rho_t]^T$ is the configuration vector of the t th segment
Ψ	$\Psi \equiv [\Psi_1^T, \Psi_2^T]^T$ is the configuration vector of the continuum arm

B. Kinematics of a Single Segment

The kinematics of a single segment depends on the rod insertion, since the insertion of the curvature-constraining rod changes the position of a segment's end ring and constrained base ring.

The t th segment possesses three DoFs, specified by the configuration vector $\Psi_t \equiv [\theta_t, \delta_t, \rho_t]^T$. Its total length, which is considered constant in this study, is l_{bt} . The length of its bent portion can then be written in (1).

$$l_{ct} = \rho_t \theta_t \quad (1)$$

The position of the t th segment's end ring, ${}^{tb}\mathbf{p}_{te}$, is written in (2).

$${}^{tb}\mathbf{p}_{te} = {}^{tb}\mathbf{p}_{tc} + {}^{tb}\mathbf{R}_{tc} {}^{tc}\mathbf{p}_{te} \quad (2)$$

Where ${}^{tb}\mathbf{R}_{tc}$ is an identity matrix since $\{tc\}$ is translated from $\{tb\}$.

${}^{tc}\mathbf{p}_{te}$ is the position of the end ring in $\{tc\}$, which is written in (3) according to a previous study [4].

$${}^{tc}\mathbf{p}_{te} = \frac{l_{ct}}{\theta_t} [\cos \delta_t (1 - \cos \theta_t) \sin \delta_t (\cos \theta_t - 1) \sin \theta_t]^T \quad (3)$$

${}^{tb}\mathbf{p}_{tc}$ is the position of $\{tc\}$ in $\{tb\}$ and depends on the length of the constrained portion as in (4):

$${}^{tb}\mathbf{p}_{tc} = [0 \ 0 \ l_{bt} - l_{ct}]^T \quad (4)$$

Substituting (1), (3) and (4) into (2) gives (5).

$${}^{tb}\mathbf{p}_{te} = \begin{bmatrix} \rho_t \cos \delta_t (1 - \cos \theta_t) \\ \rho_t \sin \delta_t (\cos \theta_t - 1) \\ \rho_t \sin \theta_t + l_{bt} - \rho_t \theta_t \end{bmatrix} \quad (5)$$

The orientation of the t th segment's end ring is written as in (6) referring to the previous study [4].

$${}^{tb}\mathbf{R}_{te} = \begin{bmatrix} \cos \theta_t (\cos \delta_t)^2 + (\sin \delta_t)^2 & \sin \delta_t \cos \delta_t (1 - \cos \theta_t) & \cos \delta_t \sin \theta_t \\ \sin \delta_t \cos \delta_t (1 - \cos \theta_t) & \cos \theta_t (\sin \delta_t)^2 + (\cos \delta_t)^2 & -\sin \delta_t \sin \theta_t \\ -\cos \delta_t \sin \theta_t & \sin \delta_t \sin \theta_t & \cos \theta_t \end{bmatrix} \quad (6)$$

The instantaneous kinematics from configuration space Ψ_t to task space \mathbf{x}_t can be formulated as:

$$\dot{\mathbf{x}}_t = \begin{bmatrix} \mathbf{v}_t^T \\ \boldsymbol{\omega}_t^T \end{bmatrix}^T = \mathbf{J}_{t\psi} \dot{\Psi}_t = \begin{bmatrix} \mathbf{J}_{t\psi}^T & \mathbf{J}_{t\omega\psi}^T \end{bmatrix}^T \dot{\Psi}_t \quad (7)$$

$$\mathbf{J}_{t\psi} = \begin{bmatrix} \rho_t \cos \delta_t \sin \theta_t & \rho_t \sin \delta_t (\cos \theta_t - 1) & \cos \delta_t (1 - \cos \theta_t) \\ -\rho_t \sin \delta_t \sin \theta_t & \rho_t \cos \delta_t (\cos \theta_t - 1) & \sin \delta_t (\cos \theta_t - 1) \\ \rho_t \cos \theta_t - \rho_t & 0 & \sin \theta_t - \theta_t \end{bmatrix} \quad (8)$$

$$\mathbf{J}_{t\omega\psi} = \begin{bmatrix} -\sin \delta_t & \cos \delta_t \sin \theta_t & 0 \\ -\cos \delta_t & -\sin \delta_t \sin \theta_t & 0 \\ 0 & \cos \theta_t - 1 & 0 \end{bmatrix} \quad (9)$$

Actuation kinematics for pushing and pulling the backbones in the PS to bend the DS to the desired configuration Ψ_t should refer to the derivations in [32].

C. Kinematics of the 2-Segment Continuum Manipulator

When the DS-2 is stacked on top of the DS-1, $\{1e\}$ coincides with $\{2b\}$. The coordinates of the 2-segment continuum arm are depicted in Fig. 7, whereas the tip position can be written as follows.

$${}^{1b}\mathbf{p}_{2e} = {}^{1b}\mathbf{p}_{1e} + {}^{1b}\mathbf{R}_{2b} {}^{2b}\mathbf{p}_{2e} \quad (10)$$

Where ${}^{1b}\mathbf{R}_{2b} \equiv {}^{1b}\mathbf{R}_{1e}$ and ${}^{2b}\mathbf{p}_{2e}$ is from (2).

The orientation of the end ring is then written as below.

$${}^{1b}\mathbf{R}_{2e} = {}^{1b}\mathbf{R}_{1e} {}^{1e}\mathbf{R}_{2b} {}^{2b}\mathbf{R}_{2e} = {}^{1b}\mathbf{R}_{1e} {}^{2b}\mathbf{R}_{2e} \quad (11)$$

Where ${}^{2b}\mathbf{R}_{2e}$ is from (6).

The instantaneous kinematics from the configuration space Ψ to the task space ${}^{1b}\mathbf{x}_2$ can be described as follows.

$${}^{1b}\dot{\mathbf{x}}_2 = \begin{bmatrix} {}^{1b}\mathbf{v}_2^T & {}^{1b}\boldsymbol{\omega}_2^T \end{bmatrix}^T = \mathbf{J} \dot{\Psi} = \mathbf{J} \begin{bmatrix} \dot{\Psi}_1^T & \dot{\Psi}_2^T \end{bmatrix}^T \quad (12)$$

Where the Jacobian matrix \mathbf{J} of the 2-segment continuum arm can be derived as below:

$$\mathbf{J} = \begin{bmatrix} \mathbf{J}_{1\psi}^T & \mathbf{J}_{2\psi}^T \end{bmatrix}^T \quad (13)$$

Where:

$$\mathbf{J}_{1\psi} = \begin{bmatrix} \mathbf{J}_{1\psi} - ({}^{1b}\mathbf{R}_{2b} {}^{2b}\mathbf{p}_{2e})^\wedge \mathbf{J}_{1\omega\psi} & {}^{1b}\mathbf{R}_{2b} \mathbf{J}_{2\psi} \end{bmatrix} \quad (14)$$

$$\mathbf{J}_{2\psi} = \begin{bmatrix} \mathbf{J}_{1\omega\psi} & {}^{1b}\mathbf{R}_{2b} \mathbf{J}_{2\omega\psi} \end{bmatrix} \quad (15)$$

Where $(\mathbf{p})^\wedge$ is the skew-symmetric matrix of the vector \mathbf{p} . $\mathbf{J}_{1\psi}$ and $\mathbf{J}_{1\omega\psi}$ are from (8) and (9) respectively.

The parameters of the 2-segment continuum arm are listed in TABLE II. Its workspace is generated as in Fig. 7 by scanning the configuration space. An unreachable volume exists inside the workspace. The points A, B and C for stiffness characterizations in Section V.B are also shown.

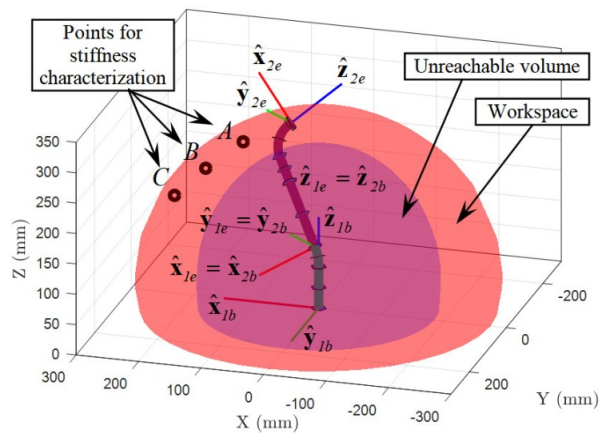


Fig. 7. Coordinates and workspace of the 2-segment continuum arm

TABLE II
PARAMETERS OF THE DISTAL SEGMENT IN THE PROTOTYPE

$l_{b1} = 100$ mm	$l_{b2} = 215$ mm	$r_{ii} = 5$ mm	$l_{ct} \in [0\text{mm}, 100\text{m}]$
$\theta_t \in [0^\circ, 135^\circ]$	$\delta_t \in [0^\circ, 360^\circ)$	$\rho_t \in [40, +\infty)$	

D. A Preliminary Stiffness Adjustment Formulation

The DSs' stiffness heavily depends on the radii of curvature $\boldsymbol{\rho} = [\rho_1 \ \rho_2]^T$. For the same bending angle, a smaller radius of curvature would lead to a higher stiffness, no matter the force is exerted within or outside the bending plane, verified by the experimental results in Section V.B.

Since the 2-segment continuum arm cannot twist, the arm cannot reach any arbitrary orientation in its workspace. Then the preliminary stiffness adjustment formulation is proposed to drive the continuum arm to reach a given target tip position with desired radii of curvature.

Rates of the arm's configuration vector $\boldsymbol{\psi}$ generate a linear velocity ${}^{lb}\mathbf{v}_2$ towards a desired target tip position according to (16). Then the rates of changes in the radii of curvature $\dot{\boldsymbol{\rho}}$ should satisfy (17) in order not to affect the linear velocity ${}^{lb}\mathbf{v}_2$. (17) gives (18), indicating that the segments should be bent according to $\dot{\boldsymbol{\psi}}_b$ to generate a desired $\dot{\boldsymbol{\rho}}$.

$${}^{lb}\mathbf{v}_2 = \mathbf{J}_{\mathbf{v}\boldsymbol{\psi}} \boldsymbol{\psi} \quad (16)$$

$$\mathbf{0} = \mathbf{J}_b \dot{\boldsymbol{\psi}}_b + \mathbf{J}_c \dot{\boldsymbol{\rho}} \quad (17)$$

Where $\boldsymbol{\Psi}_b \equiv [\theta_1 \ \delta_1 \ \theta_2 \ \delta_2]^T$, $\mathbf{J}_b = [\mathbf{J}_{\mathbf{v}\boldsymbol{\psi}}(:,1:2) \ \mathbf{J}_{\mathbf{v}\boldsymbol{\psi}}(:,4:5)]$ and $\mathbf{J}_c = [\mathbf{J}_{\mathbf{v}\boldsymbol{\psi}}(:,3) \ \mathbf{J}_{\mathbf{v}\boldsymbol{\psi}}(:,6)]$.

$$\dot{\boldsymbol{\psi}}_b = -\mathbf{J}_b^+ \mathbf{J}_c \dot{\boldsymbol{\rho}} \quad (18)$$

Where \mathbf{J}_b^+ is the pseudo inverse of the matrix \mathbf{J}_b .

During each iteration of an inverse kinematics process using the resolved rates algorithm, the continuum arm is driven from the current position towards a target position, varying the segments' radii of curvature.

Firstly, the desired velocity is obtained according to (19). Then the increment of the configuration vector $\Delta\boldsymbol{\Psi}$ is as in (20) and it is used to update the configuration vector as in (21).

$${}^{lb}\mathbf{v}_2 = v_{\text{lim}} (\mathbf{p}_{2e}^{\text{target}} - \mathbf{p}_{2e}^{\text{current}}) / \|\mathbf{p}_{2e}^{\text{target}} - \mathbf{p}_{2e}^{\text{current}}\| \quad (19)$$

Where v_{lim} is the linear velocity limit of the arm's tip.

$$\Delta\boldsymbol{\Psi} = \mathbf{J}_{\mathbf{v}\boldsymbol{\psi}}^+ {}^{lb}\mathbf{v}_2 \Delta t \quad (20)$$

Where the $\mathbf{J}_{\mathbf{v}\boldsymbol{\psi}}^+$ is the pseudo inverse of the matrix $\mathbf{J}_{\mathbf{v}\boldsymbol{\psi}}$, and Δt is the duration of the iteration.

$$\boldsymbol{\psi} = \boldsymbol{\psi} + \Delta\boldsymbol{\Psi} \quad (21)$$

Secondly the formulation drives the segments' radii of curvature towards the target values. The desired rates $\dot{\boldsymbol{\rho}}$ is obtained according to (22). Then the configuration variables ($\boldsymbol{\Psi}_b \equiv [\theta_1 \ \delta_1 \ \theta_2 \ \delta_2]^T$) are updated using (23).

$$\dot{\boldsymbol{\rho}} = \rho_{\text{lim}} (\boldsymbol{\rho}^{\text{target}} - \boldsymbol{\rho}^{\text{current}}) / \|\boldsymbol{\rho}^{\text{target}} - \boldsymbol{\rho}^{\text{current}}\| \quad (22)$$

Where ρ_{lim} is the rates limit for changing the radii of curvature.

$$\Delta\boldsymbol{\psi}_b = -\mathbf{J}_b^+ \mathbf{J}_c \dot{\boldsymbol{\rho}} \Delta t \quad (23)$$

Using this preliminary stiffness adjustment formulation, the arm is driven from $[0 \ -180 \ 210]^T$ to $[-180 \ 0 \ 210]^T$, varying the ρ_i from 40 mm to 80 mm. The simulation is shown in Fig. 8 and in the multimedia extension, where $\Delta t = 0.01\text{s}$, $v_{\text{lim}} = 20$

mm/s and $\rho_{\text{lim}} = 1.5 \text{ mm/s}$.

From the simulation it can be seen that the target position was reach first and the segments continue to change their radii of curvature. By varying the two coefficients of v_{lim} and ρ_{lim} , the position tracking and the curvature changing can be completed simultaneously. The parameters were not adjusted to demonstrate that the proposed formulation can also be used to vary the radii of curvature (a.k.a. stiffness) while maintaining its tip position.

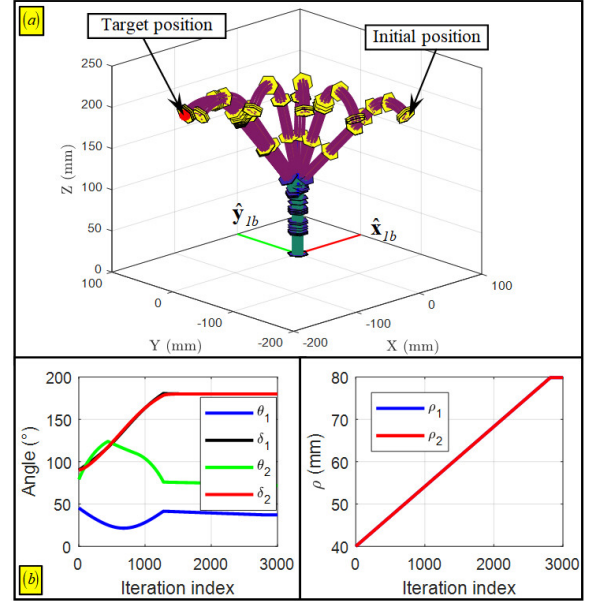


Fig. 8. Simulated position tracking while varying the stiffness: (a) poses, (b) joint trajectories (including ρ_i)

V. EXPERIMENTAL CHARACTERIZATIONS

The motion calibration is presented in Section V.A. The characterizations for the stiffness variation are presented in Section V.B.

A. Motion Calibration

The experimental setup for motion calibration refers to a previous study in [33]. Each DS was driven to bend to $\theta_i = 45^\circ$ with δ_i ranging from 0° to 360° in increments of 5° . An optical tracker (Micron Tracker SX60, Claron Technology Inc.) was used to identify the actual bending angles as shown in Fig. 9(a). The actual bending angles before motion calibration are plotted in Fig. 9(b).

The actuation compensation was formulated as follows.

$$\tilde{\theta}_i = k_i \theta_i, \quad i = 1, 2 \quad (24)$$

Where $k_1 = 1.280$ and $k_2 = 1.285$ are the compensation coefficients such that the compensated angle $\tilde{\theta}_i$ shall be used in the actuation kinematics to bend the DS to the angle θ_i .

With the compensation implemented, the bending angles θ_i varied around the desired value of 45° , as shown in Fig. 9(b). No compensation was implemented for δ_i due to the redundant arrangement of the backbones.

B. Stiffness Quantification

Stiffness of the continuum arm was quantified at different

positions with different radii of curvature of the DSs to demonstrate the effectiveness of the proposed idea. The experiments were conducted in a quasi-static condition.

The arm was driven to three positions (${}^{lb}\mathbf{p}_A$, ${}^{lb}\mathbf{p}_B$ and ${}^{lb}\mathbf{p}_C$) within its workspace as depicted in Fig. 7. At each position, three poses of the arm were tested: $\rho_t = 40$ mm, $\rho_t = 80$ mm and $l_{ct} = 100$ mm. Under the pose of $l_{ct} = 100$ mm, the curvature constraining rod will not be extended into the bendable portion of the DSs. Radii of curvature changing for the two DSs were set identical to simplify this pilot study. They can be set independently in the future studies.

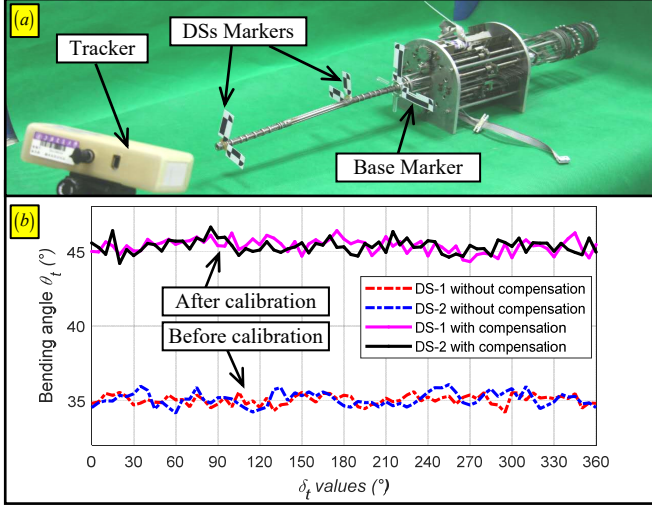


Fig. 9. Motion calibration for the continuum arm: (a) setup, and (b) bending angles of the DS-1 and DS-2 before and after the calibration

The position tracking and the radii of curvature changing were controlled using the derived formulation from Section IV.D. Different poses of the arm under the radii of curvature changing were shown in the multimedia extension.

The continuum arm was first positioned at the desired point under the aforementioned poses. A 6D force sensor (Nano-17 from ATI Industrial Automation) with a home-made probe mounted on a 3-DoF motion stage was utilized to measure the exerted force. The force sensor has a measurement range of ± 25 N in the XY directions and ± 35 N in the Z direction with 1/160 N sensing accuracy.

As shown in Fig. 10(a), the probe on the force sensor was firstly positioned by the motion stage to touch the tip of the manipulator. Then the probe was moved to perturb the tip in the $\hat{\mathbf{x}}_{lb}$, $\hat{\mathbf{y}}_{lb}$ and $\hat{\mathbf{z}}_{lb}$ directions respectively. The exerted forces were recorded for every 0.5 mm perturbation. The slope between the measured forces and the given movements can be fitted to estimate the stiffness in different directions.

The arm poses concerning the reached positions and the configuration variables ($\Psi_b \equiv [\theta_1 \delta_1 \theta_2 \delta_2]^T$) are listed in Table III. The experimental results are plotted in Fig. 10(b). The stiffness in different directions is listed above each subplot. The unit for the stiffness is N/mm.

TABLE III
ARM POSES DURING THE EXPERIMENTAL CHARACTERIZATIONS

	${}^{lb}\mathbf{p}_A = [120 \ 0 \ 260]^T$	${}^{lb}\mathbf{p}_B = [180 \ 0 \ 210]^T$	${}^{lb}\mathbf{p}_C = [230 \ 0 \ 160]^T$
$\rho_t = 40$ mm	$\Psi_b = [0.4120 \ 0 \ 1.5119 \ 0]^T$	$\Psi_b = [0.7936 \ 0 \ 1.3750 \ 0]^T$	$\Psi_b = [1.1901 \ 0 \ 0.6325 \ 0]^T$

$\rho_t = 80$ mm	$\Psi_b = [0.2943 \ 0 \ 1.2500 \ 0]^T$	$\Psi_b = [0.6468 \ 0 \ 1.2500 \ 0]^T$	$\Psi_b = [0.9949 \ 0 \ 1.0513 \ 0]^T$
$l_{ct} = 100$ mm	$\Psi_b = [0.2423 \ 0 \ 1.4702 \ 0]^T$	$\Psi_b = [0.5605 \ 0 \ 1.5477 \ 0]^T$	$\Psi_b = [0.9055 \ 0 \ 1.2166 \ 0]^T$

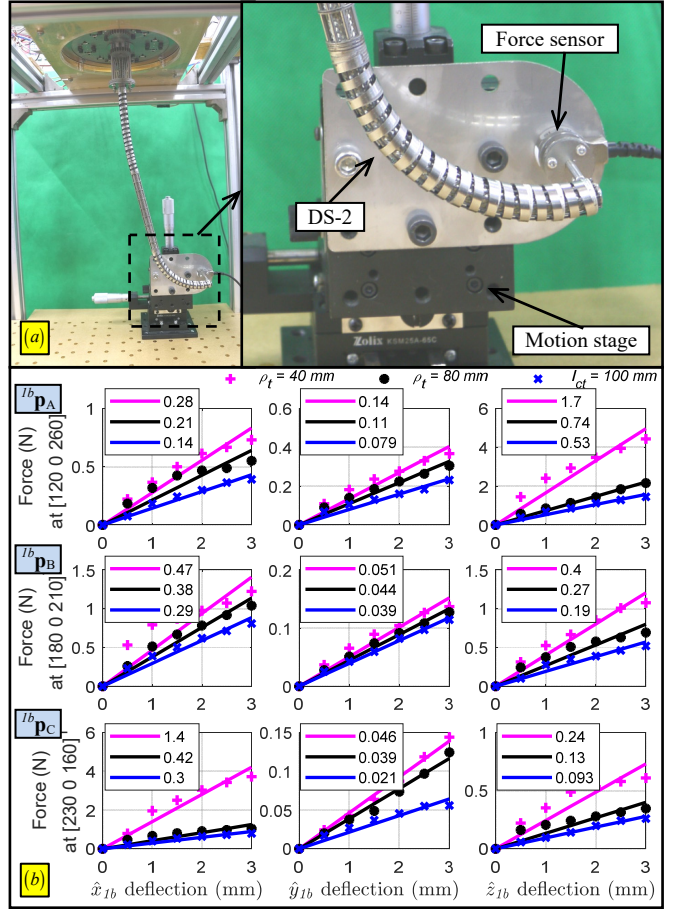


Fig. 10. Stiffness characterizations: (a) experimental setup, and (b) stiffness quantification at the three positions with the unit of N/mm

A few observations can be made from Fig. 10(b).

- It is evident that shorter ρ_t (higher curvature) generates higher stiffness. The curvature constraining rod can effectively increase the segments' stiffness. The stiffness is increased from 1.29 to 4.71 times of the values without the curvature constraining rod ($l_{ct} = 100$ mm).
- The arm's stiffness is worst in $\hat{\mathbf{y}}_{lb}$ which is perpendicular to the bending plane ($\delta_t = 0$). The reasons are on two manifolds. Firstly, the segment is inherently less stiff in the direction that is normal to the bending plane. Secondly (and more importantly), the arm does not have a structure to resist twisting. The force in $\hat{\mathbf{y}}_{lb}$ generates a large twisting moment at the base of the continuum arm, leading to a lower stiffness in $\hat{\mathbf{y}}_{lb}$.

VI. CONCLUSIONS AND FUTURE WORKS

The paper proposes a design of variable stiffness for a continuum manipulator based on redundant backbone arrangement and curvature constraining, aiming at increasing the applicability of continuum manipulators. The design concept, system construction, kinematics, preliminary stiffness adjustment and experimentation are reported.

Experimental results indicate that the arm's stiffness can be increased 4.71 times while using the curvature constraining rods. A key component, the jointed chain with minimal bending stiffness and high axial rigidity, enabled this design idea. Considering a previous study [21] where a continuum arm's stiffness was increased 4 times by redundantly arranging the backbones, the achievable stiffness variation can be as high as 18.84 times of the minimal value.

Future works mainly include two aspects. First, anti-twisting components shall be integrated to further increase the arm's apparent stiffness. Second, more complicated stiffness variation formulation shall be derived, using approaches of nonlinear mechanics modeling and/or machine learning, to independently change the configuration variables to increase the isotropy of the stiffness in different directions.

REFERENCES

- [1] J. Burgner-Kahrs, D. C. Rucker, and H. Choset, "Continuum Robots for Medical Applications: A Survey," *IEEE Transactions on Robotics*, vol. 31, No.6, pp. 1261-1280, Dec 2015.
- [2] E. Paljug, T. Ohm, and S. Hayati, "The JPL Serpentine Robot: a 12 DOF System for Inspection," in *IEEE International Conference on Robotics and Automation (ICRA)*, Washington, DC, 1995, pp. 3143-3148.
- [3] W. McMahan, V. Chitrakaran, M. Csencsits, D. M. Dawson, I. D. Walker, B. A. Jones, M. Pritts, D. Dienno, M. Grissom, and C. D. Rahn, "Field Trials and Testing of the OctArm Continuum Manipulator," in *IEEE International Conference on Advanced Robotics (ICAR)*, Orlando, FL, USA, 2006, pp. 2336-2341.
- [4] S. Liu, Z. Yang, Z. Zhu, L. Han, X. Zhu, and K. Xu, "Development of a Dexterous Continuum Manipulator for Exploration and Inspection in Confined Spaces," *Industrial Robot: An International Journal*, vol. 43, No.3, pp. 284-295, 2016.
- [5] I. D. Walker, "Continuous Backbone "Continuum" Robot Manipulators," *ISRN Robotics*, vol. 2013, No.726506, pp. 1-19, 2013.
- [6] T.-D. Nguyen and J. Burgner-Kahrs, "A Tendon-Driven Continuum Robot with Extensible Sections," in *IEEE/RSJ International Conference on Intelligent Robots and Systems (IROS)*, Hamburg, Germany, 2015, pp. 2130-2135.
- [7] V. Saadat, R. C. Ewers, and E. G. Chen, "Shape Lockable Apparatus and Method for Advancing an Instrument through Unsupported Anatomy," US: USGI Medical, Inc., 2004.
- [8] L. L. Swanstrom, R. Kozarek, P. J. Pasricha, S. Gross, D. Birkett, P.-O. Park, V. Saadat, R. Ewers, and P. Swain, "Development of a New Access Device for Transgastric Surgery," *Journal of Gastrointestinal Surgery*, vol. 9, No.8, pp. 1129-1137, 2006.
- [9] A. Degani, H. Choset, A. Wolf, and M. A. Zenati, "Highly Articulated Robotic Probe for Minimally Invasive Surgery," in *IEEE International Conference on Robotics and Automation (ICRA)*, Orlando, Florida, 2006, pp. 4167- 4172.
- [10] Y.-J. Kim, S. Cheng, S. Kim, and K. Iagnemma, "A Stiffness-Adjustable Hyperredundant Manipulator Using a Variable Neutral-Line Mechanism for Minimally Invasive Surgery," *IEEE Transactions on Robotics*, vol. 30, No.2, pp. 382-395, April 2014.
- [11] P. M. Loschak, S. F. Burke, E. Zumbro, A. R. Forelli, and R. D. Howe, "A Robotic System for Actively Stiffening Flexible Manipulators," in *IEEE/RSJ International Conference on Intelligent Robots and Systems (IROS)*, Hamburg, Germany, 2015, pp. 216-221.
- [12] A. Yagi, K. Matsumiya, K. Masamune, H. Liao, and T. Dohi, "Rigid-Flexible Outer Sheath Model Using Slider Linkage Locking Mechanism and Air Pressure for Endoscopic Surgery," in *International Conference on Medical Image Computing and Computer-Assisted Intervention (MICCAI)*, Copenhagen, Denmark, 2006, pp. 503-510.
- [13] A. J. Loeve, O. S. v. d. Ven, J. G. Vogel, P. Breedveld, and J. Dankelman, "Vacuum Packed Particles as Flexible Endoscope Guides with Controllable Rigidity," *Granular Matter*, vol. 12, No.6, pp. 543-554, 2010.
- [14] N. G. Cheng, M. B. Lobovsky, S. J. Keating, A. M. Setapen, K. I. Gero, A. E. Hosoi, and K. D. Iagnemma, "Design and Analysis of a Robust, Low-cost, Highly Articulated Manipulator Enabled by Jamming of Granular Media," in *IEEE International Conference on Robotics and Automation (ICRA)*, Saint Paul, Minnesota, USA, 2012, pp. 4328-4333.
- [15] Y.-J. Kim, S. Cheng, S. Kim, and K. Iagnemma, "A Novel Layer Jamming Mechanism With Tunable Stiffness Capability for Minimally Invasive Surgery," *IEEE Transactions on Robotics*, vol. 29, No.4, pp. 1031-1042, Aug 2013.
- [16] A. Petersson, S. Davis, J. O. Gray, T. J. Dodd, and T. Ohlsson, "Design of a Magnetorheological Robot Gripper for Handling of Delicate Food Products with Varying Shapes," *Journal of Food Engineering*, vol. 98, No.3, pp. 332-338, June 2010.
- [17] A. Sadeghi, L. Beccai, and B. Mazzolai, "Innovative Soft Robots Based on Electro-Rheological Fluids," in *IEEE/RSJ International Conference on Intelligent Robots and Systems (IROS)*, Vilamoura, Algarve, Portugal, 2012, pp. 4237-4242.
- [18] M. J. Telleria, M. Hansen, D. Campbell, A. Servi, and M. L. Culpepper, "Modeling and Implementation of Solder-activated Joints for Single-Actuator, Centimeter-scale Robotic Mechanisms," in *IEEE International Conference on Robotics and Automation (ICRA)*, Anchorage, Alaska, USA, 2010, pp. 1681-1686.
- [19] W. Shan, T. Lu, and C. Majidi, "Soft-matter Composites with Electrically Tunable Elastic Rigidity," *Smart Materials and Structures*, vol. 22, No.085005, pp. 1-8, July 2013.
- [20] M. L. Fugoso and D. H. Tran, "Adjustable Stiffness Dilatation Catheter," US: Medtronic, Inc., 1996.
- [21] B. L. Conrad, J. Jung, R. S. Penning, and M. R. Zinn, "Interleaved Continuum-Rigid Manipulation: An Augmented Approach for Robotic Minimally-Invasive Flexible Catheter-Based Procedures," in *IEEE International Conference on Robotics and Automation (ICRA)*, Karlsruhe, Germany, 2013, pp. 718-724.
- [22] K. Xu, M. Fu, and J. Zhao, "An Experimental Kinesthetic Comparison between Continuum Manipulators with Structural Variations," in *IEEE International Conference on Robotics and Automation (ICRA)*, Hong Kong, China, 2014, pp. 3258-3264.
- [23] M. Mahvash and P. E. Dupont, "Stiffness Control of Surgical Continuum Manipulators," *IEEE Transactions on Robotics*, vol. 27, No.2, pp. 334-345, April 2011.
- [24] D. C. Rucker and R. J. Webster, "Statics and Dynamics of Continuum Robots With General Tendon Routing and External Loading," *IEEE Transactions on Robotics*, vol. 27, No.6, pp. 1033-1044, Dec 2011.
- [25] İ. Tunay, "Spatial Continuum Models of Rods Undergoing Large Deformation and Inflation," *IEEE Transactions on Robotics*, vol. 29, No.2, pp. 297-307, April 2013.
- [26] W. S. Rone and P. Ben-Tzvi, "Continuum Robot Dynamics Utilizing the Principle of Virtual Power," *IEEE Transactions on Robotics*, vol. 30, No.1, pp. 275-287, Feb 2014.
- [27] A. Bajo and N. Simaan, "Hybrid Motion/Force Control of Multi-Backbone Continuum Robots," *International Journal of Robotics Research*, vol. OnlineFirst, pp. 1-13, 2015.
- [28] K. Xu and N. Simaan, "An Investigation of the Intrinsic Force Sensing Capabilities of Continuum Robots," *IEEE Transactions on Robotics*, vol. 24, No.3, pp. 576-587, June 2008.
- [29] K. Xu and N. Simaan, "Intrinsic Wrench Estimation and Its Performance Index of Multi-Segment Continuum Robots," *IEEE Transactions on Robotics*, vol. 26, No.3, pp. 555-561, June 2010.
- [30] K. Xu and N. Simaan, "Analytic Formulation for the Kinematics, Statics and Shape Restoration of Multibackbone Continuum Robots via Elliptic Integrals," *Journal of Mechanisms and Robotics*, vol. 2, No.011006, pp. 1-13, Feb 2010.
- [31] Z. Li, H. Ren, P. W. Y. Chiu, R. Du, and H. Yu, "A Novel Constrained Wire-Driven Flexible Mechanism and Its Kinematic Analysis," *Mechanism and Machine Theory*, vol. 95, pp. 59-75, Jan 2016.
- [32] K. Xu, J. Zhao, and M. Fu, "Development of the SJTU Unfoldable Robotic System (SURS) for Single Port Laparoscopy," *IEEE/ASME Transactions on Mechatronics*, vol. 20, No.5, pp. 2133-2145, Oct 2015.
- [33] K. Xu and N. Simaan, "Actuation Compensation for Flexible Surgical Snake-like Robots with Redundant Remote Actuation," in *IEEE International Conference on Robotics and Automation (ICRA)*, Orlando, Florida, USA, 2006, pp. 4148- 4154.